Performance of Shunt Active Power Filter Based on Instantaneous Reactive Power Control Theory for Single-Phase System

D. M. Soomro*, S. C. Chong**‡, Z. A. Memon***, M. A. Uqaili****, F. Abbasi*****

*Department of Electrical Power Engineering, Faculty of Electrical and Electronic Engineering, University Tun Hussein Onn Malaysia, 86400 Parit Raja, Johor, Malaysia.

**Department of Electrical Power Engineering, Faculty of Electrical and Electronic Engineering, University Tun Hussein Onn Malaysia, 86400 Parit Raja, Johor, Malaysia.

***Department of Electrical Engineering, Mehran University of Electrical Power Engineering, Jamshoro, Pakistan.

****Department of Electrical Engineering, Mehran University of Electrical Power Engineering, Jamshoro, Pakistan.

*****Quaid-e-Awam University of Engineering Science and Technology, Larkana, Sindh, Pakistan.

(dursoomro@uthm.edu.my, tamama_chin@yahoo.com.my, zubair.memon@faculty.muet.edu.pk, vc@admin.muet.edu.pk, farhan.abbasi@quest.edu.pk)

‡ S. C. Chong, Tel: +60 17 5105536, tamama_chin@yahoo.com.my

Received: 31.03.2017 Accepted: 16.07.2017

Abstract- Recently more aware people had more concern on the quality of power supply. One of the reasons is due to the increasing demand of nonlinear loads. One of the major power quality (PQ) problems that causing malfunction of sensitive electronic equipment is harmonics. The Instantaneous Reactive Power (IRP) theory is the method that is used to calculate the harmonic compensation current for three-phase system. This technique is commonly used in the shunt active power filter (APF) for reducing the harmonics and providing a good harmonic compensation for unbalanced and nonlinear load conditions. This control theory will treat the three-phase system as three single-phase system. Therefore, it also can be implemented in the single-phase system. Implementation of IRP theory for single-phase system can be done by using two methods, which are Clarke's transformation method and Phase-shift method. The aim of this paper is to discuss the performance shunt APF based on IRP theory for single-phase power system based on Clarke's transformation method and Phase-shift method to compensate current harmonics generated by nonlinear loads in MATLAB/Simulink to show the effectiveness of the tested control methods. Results show, that Clarke's transformation method has better harmonics compensation ability compared to Phase-shift method, it able to compensate odds and even harmonics.

Keywords Active filter, control system, load modelling, harmonic, nonlinear load.

1. Introduction

The increasing of harmonics in power system (PS) is caused by the connected nonlinear loads and usage of power converter at the end-user. Many of harmonic sources are single-phase loads such as computer, fluorescent lamp, LED lamps, charger, printer and other home electronic equipments [1, 2]. Mostly, the home electronic appliances implement rectifier circuit for providing DC supply to the loads. The rectification will drag the current to non-linearity from the power supply and causes harmonic injection in the power supply [3]. Moreover, the power converters are used in industry to control the manufacturing processes and machines or the renewable energy like solar PV and wind that connected with the grid also are the source of harmonics [4-6].

The usage of nonlinear loads is unavoidable in the PS, but the harmonics in the PS can be mitigated by two techniques. Firstly, by be including the harmonic mitigation design precautions during the early stage of the project like segregation of harmonic producing loads from sensitive

loads, using an isolation transformer (star/delta) and selection of the variable frequency drives [7]. However, to mitigate the harmonic for existing facilities can be done by using AC line reactors, DC reactors, K-factor transformers, multi-pulse drives or power filter like passive, active, and hybrid power filter [7, 8]. But, AC line reactors and DC line reactors are less effective in reducing the harmonic current to meet the harmonic standards (i.e THD < 5 %). Moreover, using K-factor transformer it can withstand some percentage of connected nonlinear loads at the secondary winding but it is not able to reduce the system harmonics [9]. Therefore, power filter became a better solution to implement for the harmonics reduction in PS.

Initially passive filter was invented to mitigate the harmonic distortion problem. Since, the passive filter is designed to solve certain order of harmonics so it will be less effective when the system load is variable. Moreover, if the PS connect several passive filter for mitigate different order of harmonics, it may causes the resonance [10, 11]. Therefore, the APF is designed to overcome such drawback [12, 13]. For reducing current harmonic shunt APF topology is implemented [14-16]. The shunt APF is connected in parallel with the nonlinear load. The connection of shunt APF in PS is as shown in Fig. 1.

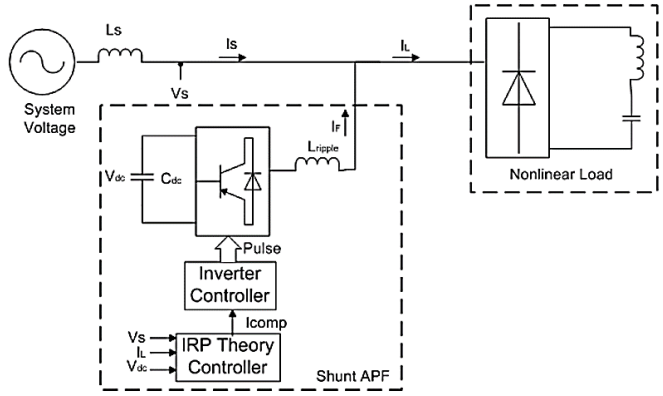

Fig. 1. Connection of shunt APF in PS.

The voltage source inverter (VSC) is implemented in the shunt APF and connected with a DC-link capacitor (C_{DC}). The function of C_{DC} in APF is to provide the reactive power that is need to compensate harmonics. The basic operation of shunt APF required current and voltage sensors for sensing AC current and voltage flow on the line and DC-link voltage at the inverter. The control system will calculate the error (harmonic current) based on the control theory which depends on the measured AC current, voltage and DC-link voltage at the inverter. The switching device in VSC provide switching pulse according to the harmonic compensation that is calculated by the IRP theory controller. A series inductor (L_{ripple}) is connected with the shunt APF to reduce the ripple in harmonic compensate reactive current.

This paper presents the modeling of a single-phase shunt APF with the control scheme based on the IRP theory for single-phase power system in MATLAB/Simulink. The simulation was carried out by using different types of loads to observe the performance of an APF.

2. Instantaneous Active and Reactive Power Theory

The IRP theory was introduced by Hirofumi Akagi in the year 1983 for three-phase circuits for define a set of instantaneous power in the time domain[17, 18]. This control theory has been widely used for harmonic compensation generated by nonlinear loads in APF for three-phase system. Most of the previous researchers [19-22] had implemented the IRP theory for single-phase systems by using Clarke's transformation and given a good harmonic compensation. Since Clarke's transformation required three-phase signals, so for implementing this method for single-phase system, the voltage and load current signals needed to be transformed into three-phase by signal shifting at ±120º [23]. However, another method named Phase-shift method can be used for IRP theory for single-phase system [24, 25]. The main advantage of Phase shift method is that there is no need of transforming the single-phase voltage and load current into three-phase form, therefore the control system is much more simplified. While, Clark's transformation provides more accuracy to get harmonic compensation current (HCC).

In the next part, we will discuss the mathematic model that has been implemented with IRP theory in single-phase system by using two methods: Method 1 (M1) Clarke's transformation and Method 2 (M2) Phase-shift method. The phase locked loop (PLL) and hysteresis current controller will also implement in both methods 1 & 2 control system. The PLL is used in the control system to make sure that the collected source voltage is at the correct phase angle. The output of PLL is unity and contains synchronizing signal sin (ωt) and cos (ωt). For IRP theory, only sin (ωt) signal will be implemented in M1 and M2 control system. The hysteresis current controller is used to make sure the switches of the inverter are follows the calculated reference current [26-28].

2.1. Method 1 – Clarke's Transformation

Before applying IRP theory with Clarke's transformation method for single-phase system, firstly it need to transform single-phase supply voltage and load current from V and I_L to three-phase V_{abc} and I_{Labc} form respectively. The measured single-phase voltage is represented in (1):

$$V = V_m \sin(\omega t) \tag{1}$$

Eq. (1) will be fed into PLL block to obtain stable sinusoidal signal with amplitude of unity [29, 30]. The output of PLL sin (ωt) signal will be used for generating the V_{abc} signals. Eq. (2), Eq. (3) and Eq. (4) show the setting for phases *abc* delay for the output signal:

$$V_a = \sin(\omega t) \tag{2}$$

$$V_b = \sin(\omega t - 120^o) \tag{3}$$

$$V_c = \sin(\omega t - 240^o) \tag{4}$$

Multiplying the peak amplitude of fundamental input voltage magnitude with V_{abc} signal from Eq. (2), Eq. (3) and Eq. (4) will give the stable voltage signals $V^*_{a,b,c}$ as shown in Eq. (5):

$$V^{*}_{a,b,c} = V_m * V_{a,b,c} \quad (5)$$

Then the system voltage became:

$$v^{*}_{a} = V_m \sin(\omega t) \quad (6)$$

$$v^{*}_{b} = V_m \sin(\omega t - 120^{\circ}) \quad (7)$$

$$v^{*}_{c} = V_m \sin(\omega t - 240^{\circ}) \quad (8)$$

In case of nonlinear load, the load current can be represented as:

$$i_{La} = \sum_{n=1}^{\infty} I_n \sin(n\omega t + \theta_n) \quad (9)$$

Assuming that this current from "i_{La}" is the phase "a" current. Similarly, the corresponding phase "b" and "c" currents can be obtain by delay ±120º, which are represented as:

$$i_{Lb} = \sum_{n=1}^{\infty} I_n \sin(n\omega t + \theta_n - 120^{\circ}) \quad (10)$$

$$i_{Lc} = \sum_{n=1}^{\infty} I_n \sin(n\omega t + \theta_n + 120^{\circ}) \quad (11)$$

These $v^{*}_{a,b,c}$ voltage signal and i_{Labc} load current signal will be send to Clarke's transformation to transform the three-phase voltages and load currents from abc plane into αβ0 coordinates as follows:

$$\begin{pmatrix} v_0 \\ v_\alpha \\ v_\beta \end{pmatrix} = \sqrt{2/3} \begin{pmatrix} 1/\sqrt{2} & 1/\sqrt{2} & 1/\sqrt{2} \\ 1 & -1/2 & -1/2 \\ 0 & \sqrt{3}/2 & -\sqrt{3}/2 \end{pmatrix} \begin{bmatrix} v^{*}_a \\ v^{*}_b \\ v^{*}_c \end{bmatrix} \quad (12)$$

$$\begin{pmatrix} i_0 \\ i_\alpha \\ i_\beta \end{pmatrix} = \sqrt{2/3} \begin{pmatrix} 1/\sqrt{2} & 1/\sqrt{2} & 1/\sqrt{2} \\ 1 & -1/2 & -1/2 \\ 0 & \sqrt{3}/2 & -\sqrt{3}/2 \end{pmatrix} \begin{bmatrix} i_{La} \\ i_{Lb} \\ i_{Lc} \end{bmatrix} \quad (13)$$

The transformation of three-phase voltage and load current from Eq. (12) and Eq. (13) will used to calculate the instantaneous zero sequence power (p_0), real (p) and instantaneous reactive power (q) as given as in Eq. (14):

$$\begin{bmatrix} p_0 \\ p \\ q \end{bmatrix} = \begin{bmatrix} v_0 & 0 & 0 \\ 0 & v_\alpha & v_\beta \\ 0 & -v_\beta & v_\alpha \end{bmatrix} \begin{bmatrix} i_0 \\ i_\alpha \\ i_\beta \end{bmatrix} \quad (14)$$

The calculated p from (14) is the total active power of the system included the power used by the average value of the instantaneous real power (p) and is transferred from the power source to the load ($\bar{p}$), the oscillating power ($\tilde{p}$) in the system. Therefore, it can be write as:

$$p = \bar{p} + \tilde{p} \quad (15)$$

The $\bar{p}$ value can be obtained by a Low Pass Filter (LPF) on the p signal. Then, the $\tilde{p}$ signal can be represented as Eq. (16):

$$\tilde{p} = p - \bar{p} \quad (16)$$

The power loss in the power inverter in APF is also refer as the regulation power (p_{reg}). The p_{reg} can be obtain by using Proportional Integral (PI) controller as a result of the error between the reference voltage (v_{ref}) and the measured DC-link voltage (v_{dc}) Eq. (17):

$$p_{reg} = k_p(v_{ref} - v_{dc}) + k_I \int (v_{ref} - v_{dc})dt \quad (17)$$

Thus, the compensation real power (p_{comp}) for the APF is given by Eq. (18):

$$p_{comp} = (p - \bar{p}) - p_{reg} = \tilde{p} - p_{reg} \quad (18)$$

The reactive power compensation (q_{comp}) is same as the calculated q. So, the αβ current references of the compensator for harmonic elimination are given as:

$$\begin{bmatrix} i_{C\alpha} \\ i_{C\beta} \end{bmatrix} = \frac{1}{v_\alpha^2 + v_\beta^2} \begin{bmatrix} v_\alpha & v_\beta \\ v_\beta & -v_\alpha \end{bmatrix} \begin{bmatrix} p_{comp} \\ q_{comp} \end{bmatrix} \quad (19)$$

The compensation currents from (19) can be transformed in abc quantities with inverse Clarke's transformation in Eq. (20):

$$\begin{bmatrix} i^{*}_{Ca} \\ i^{*}_{Cb} \\ i^{*}_{Cc} \end{bmatrix} = \sqrt{2/3} \begin{pmatrix} 1/\sqrt{2} & 1 & 0 \\ 1/\sqrt{2} & -1/2 & \sqrt{3}/2 \\ 1/\sqrt{2} & -1/2 & -\sqrt{3}/2 \end{pmatrix} \begin{pmatrix} -i_0 \\ i_{C\alpha} \\ i_{C\beta} \end{pmatrix} \quad (20)$$

For single-phase system, only the i^{*}_{Ca} is used to compensate the harmonic distortion. The i^{*}_{Ca} represent as:

$$i^{*}_{Ca} = -\frac{1}{\sqrt{3}} i_0 + i_{C\alpha} = -\frac{1}{\sqrt{3}} i_0 + \frac{v_\alpha * p_{comp} + v_\beta * q_{comp}}{v_\alpha^2 + v_\beta^2} \quad (21)$$

For single-phase system, only the i^{*}_{Ca} signal Eq. (21) will used to generate the switching pulse for the APF inverter. This i^{*}_{Ca} signal will be sent to hysteresis current controller for generating the proper switching pulse for the APF power inverter. The block diagram of this M1 controller as shown in Fig. 2.

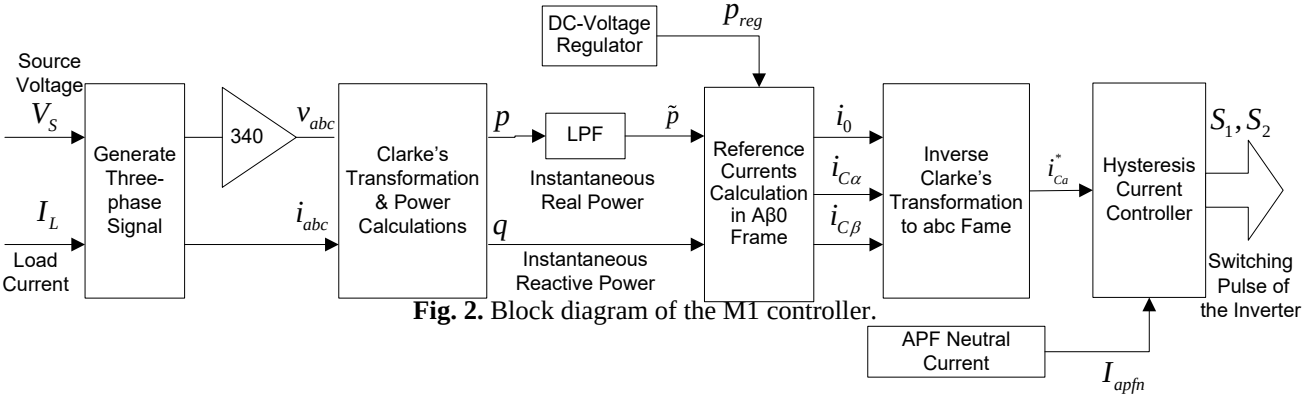

Fig. 2. Block diagram of the M1 controller.

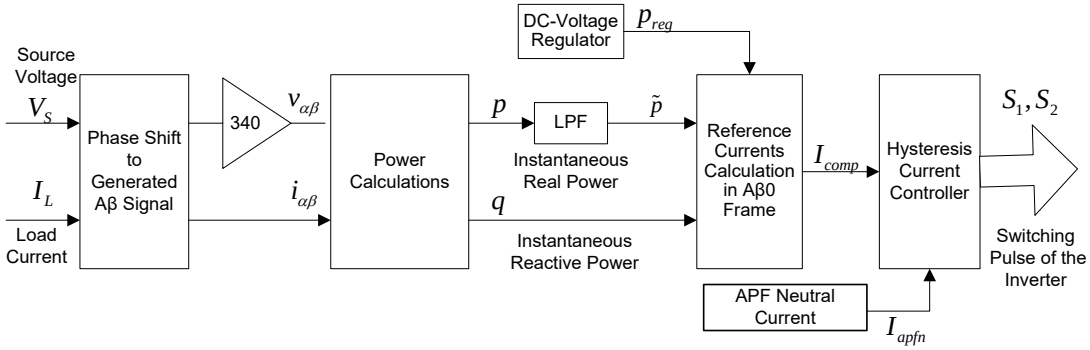

Fig. 3. Block diagram of the M2 controller.

2.2. Method 1 – Phase-shift

The PLL is also use in phase shift method to keep the source voltage synchronous with the grid voltage. Since the output signal of the PLL is unity, so it will be multiplying with the peak amplitude of fundamental input voltage magnitude (V_m) thus by given the source voltage represented as Eq. (22):

$$V_s = V_m \sin(\omega t) \tag{22}$$

The $v_{\alpha\beta}$ frame is same as the system voltage while v_β frame is phase shifted at 90º of v_α. Thus, the v_α and v_β are represented as Eq. (23) and Eq. (24):

$$v_\alpha = V_m \sin(\omega t) \tag{23}$$

$$v_\beta = v_\alpha e^{-j90°} \tag{24}$$

The load current in $i_{\alpha\beta}$ frame also can be determined by using phase shift method same as the voltage. The i_α and i_β are represented in Eq. (25) and Eq. (26):

$$i_\alpha = I_{La} = \sum_{n=1}^{\infty} I_n \sin(n\omega t + \theta_n) \tag{25}$$

$$i_\beta = I_\alpha e^{-j90°} \tag{26}$$

Hence, the p and q of the system can be calculated by using Eq. (27) and Eq. (28):

$$p = v_\alpha i_\alpha + v_\beta i_\beta \tag{27}$$

$$q = v_\alpha i_\beta - v_\beta i_\alpha \tag{28}$$

The calculated p from Eq. (26) also contains the average instantaneous real power ($\overline{p}$), the oscillating power ($\tilde{p}$) and the regulation power (p_{reg}) as same as in M1. Thus, the compensation real power (p_{comp}) for the APF is alike the Eq. (18). The reactive power compensation (q_{comp}) is similar to the calculated q. So, the compensation current (i_{comp}) can be determine by Eq. (29):

$$i_{comp} = \frac{v_\alpha * p_{comp} - v_\beta * q_{comp}}{v_\alpha^2 + v_\beta^2} \tag{29}$$

This i_{comp} will added to the hysteresis current controller for generating switching pulse for the APF power inverter to compensate the system harmonics. The block diagram of the M2 controller as shown in Fig. 3.

3. Design Parameters of Shunt APF and Nonlinear Loads

The supply voltage and frequency of a single-phase power system is 240 V and 50 Hz respectively. However, the APF DC bus reference voltage, $V_{DC,ref}$ can be determined by using the equation below [31, 32]:

$$V_{DC,min} \geq \frac{V_L}{\sqrt{2}\, m} \tag{30}$$

$$V_{DC,max} \geq \frac{2\sqrt{2}\, V_L}{\sqrt{3}\, m} \tag{31}$$

Where

V_L single-phase voltage;
m amplitude modulation index.

The m is considered as 1, assume that the inverter DC-link voltage had the same amplitude with the system peak voltage. By using (30) and (31), the calculated $V_{DC,min}$ and $V_{DC,max}$ value are set as 170 V and 400 V respectively. The DC link capacitor can be calculated by using the expression [33]:

$$\frac{1}{2} C_{DC} \left[\left(V_{DC,max}\right)^2 - \left(V_{DC,min}\right)^2 \right] = V_L (a\ I)\ t \tag{32}$$

Where

a overloading factor;
I phase current supply by the source to the load;
t time in which DC bus voltage is recovered.

The a is selected from its range of 120-180 % of steady-state current during transient condition, it is selected the maximum value is 1.8. Therefore, the calculated C_{DC} value will 329 µF for 5 A current rating at 10 ms. So, the chosen C_{DC} value is 330 µF. The selection of the coupling inductance L_{ripple} can be determine by [34, 35]:

$$L_{min} \geq \frac{\Delta V}{\omega * I_{max}} \tag{33}$$

Where

$\Delta V = V_S - V_{DC,min}$;
$\omega = 2\pi f_s$;
I_{max} maximum current.

For 5 A current rating APF, the calculated minimum inductance value is 45 mH, so 50 mH is selected. The PI

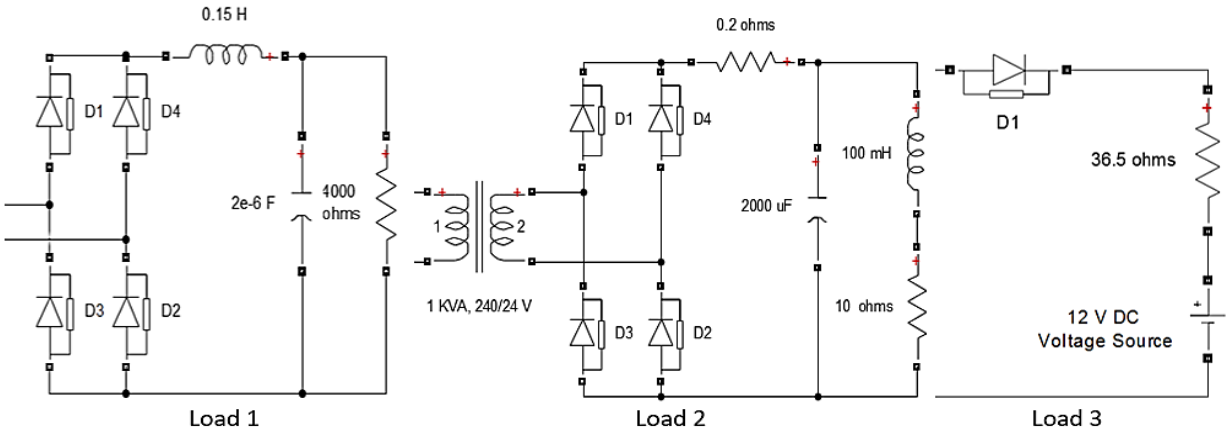

Fig. 4. Circuit model of nonlinear loads.

controller is function to control the stability of capacitor on DC side, so the value of k_p and k_i value is adjusted to obtain the stability of capacitor voltage [36]. The circuit parameters for both M1 and M2 have same setting as shown in Table 1.

Three types of non-linear loads are simulated with M1 and M2 of the single-phase IRP theory as shown in Fig. 4. Load 1 (L1), Load 2 (L2) and Load 3 (L3) are circuit model of LED lamps [37], computer model [1] and battery charger [38] respectively. L1 and L2 are supplied by a full-wave rectifier circuit and L3 is supplied by a diode. These nonlinear loads possess difference current ratings and different current total harmonic distortion (THD_I).

Table 1. Circuit parameters of the simulation model

Parameters	Values
Supply voltage,V_S	240 V
Supply frequency, f_s	50 Hz
DC bus reference voltage, $V_{DC,ref}$	400 V
APF inductance, L_{ripple}	50 mH
APF DC-link capacitor, C_{DC}	330 µF
APF PI controller	k_p=0.1, k_i=0.01

Figure 5, Fig. 6 and Fig. 7 show the current and harmonics spectrum of the nonlinear loads. The L1 and L2 had high value of odd harmonics (3rd, 5th, 7th and 9th). However, only L3 only used half-wave rectification so have high value of even harmonics (2nd, 4th and 6th). This outcome will enable to visualize the performance of the designed shunt APF in different loads conditions.

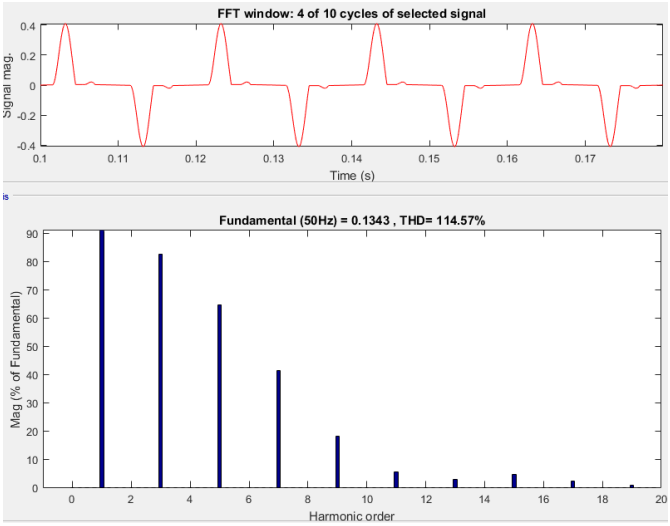

Fig. 5. L1 current and harmonics spectrum.

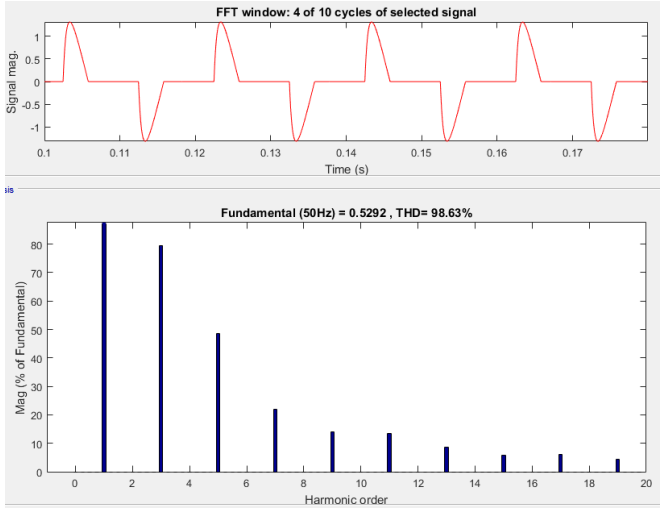

Fig. 6. L2 current and harmonics spectrum.

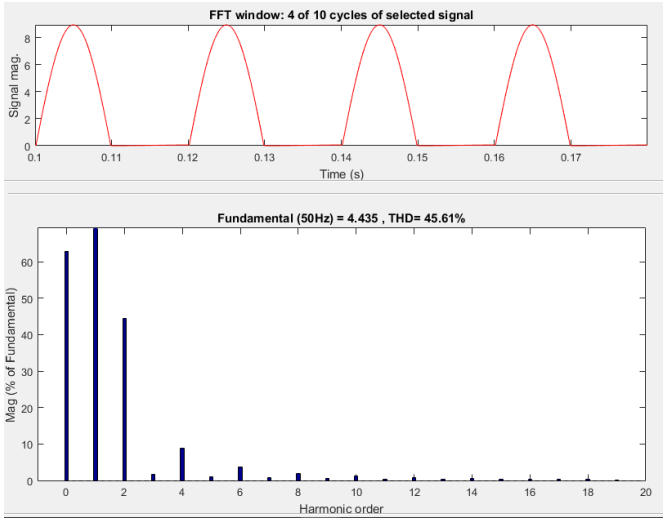

Fig. 7. L3 current and harmonics spectrum.

4. Simulation Results

Figure8 below shows the simulation circuit of the shunt APF with the nonlinear load. Table 2 shows the comparison of simulated results of the L1 and L2 in for without and with shunt APF condition apply in M1 and M2. Table 3 shows the comparison simulation results of the L3 in without and with shunt APF applied in M1 and M2.

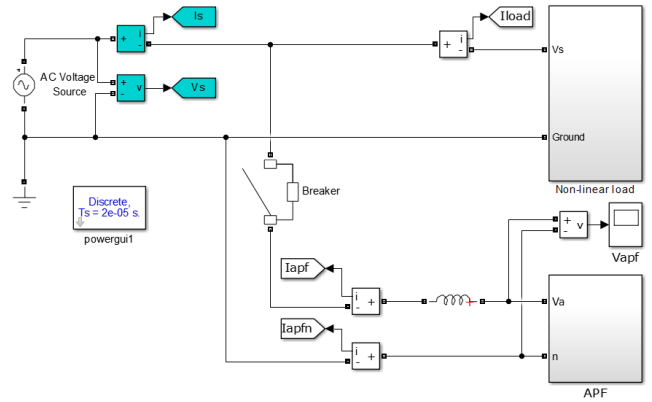

Fig. 8. Simulation model of shunt APF with non-linear load.

According to Table 2, it can observed that the M1 IRP theory gives better harmonic compensation compared to M2 for L1 and L2. Fig. 9 and Fig. 10 shows the simulation results of the collected line current waveforms with and without shunt APF for M1 and M2. By using M1, the THD_I of L1 and L2 have been reduce from 114.57 % and 98.67 % to 8.41 % and 7.17 % respectively. Still the THD_I is higher than the permissible value (i.e. $THD_I \leq 5$ %) as recommended in IEEE-519 and IEC 61000-3-2 harmonic standards [39, 40]. This condition is due to the current ratings of L1 and L2 are very low, while the IRP control theory of APF is designed for higher current rating of load. So, the ripple contained in the line current degrades the performance of APF causing the increase in THD_I value even if the current waveform remain sinusoidal.

Table 2. Simulation results for L1 and L2 without and with shunt APF Applied in M1 and M2

	L1			L2		
		After			After	
	Before	**M1**	**M2**	**Before**	**M1**	**M2**
I_{fund}, A	0.134	0.139	0.183	0.529	0.555	0.579
I_{rms}, A	0.095	0.099	0.129	0.374	0.392	0.409
THD_I, %	**114.57**	**8.41**	**34.45**	**98.63**	**7.17**	**18.82**
3rd, %	82.69	1.73	18.07	79.60	5.02	12.78
5th, %	64.74	4.99	19.23	48.62	1.48	10.16
7th, %	41.32	2.87	2.78	21.90	1.41	2.48
9th, %	18.04	2.29	3.26	14.09	0.61	1.64
11th, %	5.39	1.57	8.19	13.53	1.08	1.37
13th, %	2.94	1.50	2.16	8.63	0.79	1.08
15th, %	4.67	0.59	0.54	5.82	1.18	2.75
17th, %	2.12	2.11	2.40	6.13	0.46	4.16
19th, %	0.65	1.16	3.01	4.45	1.23	3.99

For M2 the THD_I for L1 and L2 merely reduces to 34.45 % and 18.82 % respectively. This is due to the high ripple in the compensating harmonic current. Similarly M2 is not suitable for low current rating of nonlinear loads. From Fig. 9 and Fig. 10 it is evident that M1 produces less ripple than M2.

Table 3. Simulation results for L3 without and with shunt APF Applied in M1 and M2

	L3		
		After	
	Before	**M1**	**M2**
I_{fund}, A	4.435	4.500	4.518
I_{rms}, A	3.136	3.182	3.194
THD_I, %	**45.62**	**0.88**	**36.13**
2nd, %	44.46	0.20	35.38
3rd, %	1.67	0.29	0.11
4th, %	8.81	0.26	1.84
5th, %	1.00	0.23	0.35
6th, %	3.72	0.44	0.83
7th, %	0.71	0.03	0.21
8th, %	2.02	0.21	0.25
9th, %	0.55	0.06	0.13
10th, %	1.25	0.05	0.30

From Table 3, it can be concluded that M1 provide acceptable harmonic compensate for higher power rating of L3, where it is reduced from 45.62 % to 0.88 %. Moreover, the HCC ripple is also reduce as shown in Fig. 11. Therefore, it can concluded that the designed shunt APF control system is more appreciable for high power rating of loads and can be used for three-phase system load. Additionally, the result shown in Table 3 depicts that M2 is not effective while dealing with the even harmonics. From the collected results, it is clear that the M2 is not able to reduce 2nd order harmonic. It causes distort the current waveform to be non-sinusoidal.

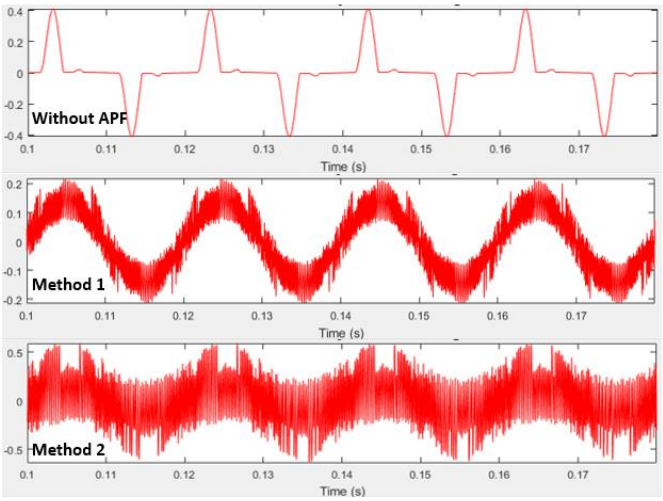

Fig. 9. L1 line current simulation waveforms.

5. Performance of Shunt APF on M1 and M2

The performance of shunt APF based on M1 and M2 shows different harmonic compensation abilities. This is due to the generated load current and the value of p and q obtained through Eq. (14). Where p_0 is omitted because of zero sequence power and is not used. Table 4 shows the collected THD_I without and with shunt APF for M1 & M2.

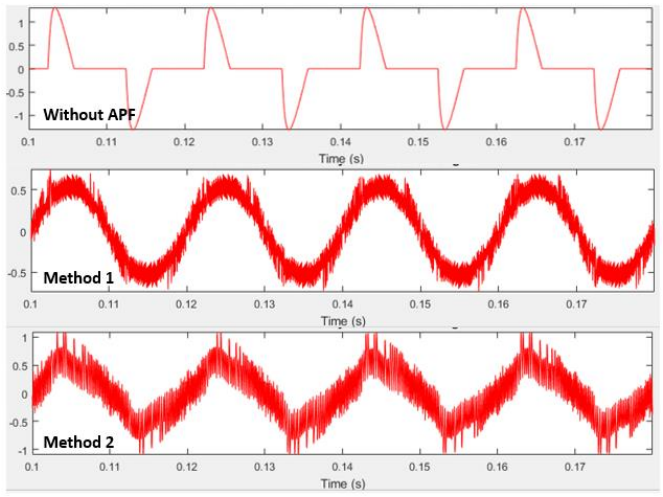

Fig. 10. L2 line current simulation waveforms.

From Table 4, the collected simulation results show that M1 is giving better harmonic compensation compared to M2 in all level of current ratings of nonlinear loads. Moreover it provides attractive compensation for both odd & even harmonics. This is due to the generated $I_{L\alpha\beta}$ of M2, causing the calculated p and q value (with less accuracy) when needed to compensate a high THD and the load generating even harmonics.

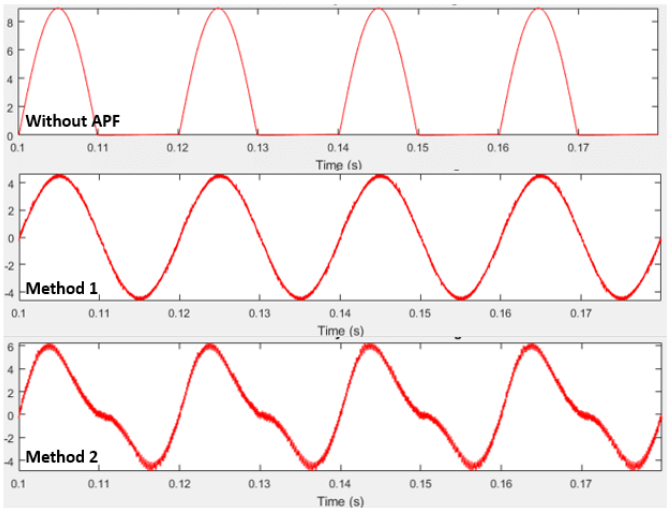

Fig. 11. L3 line current simulation waveforms.

Table 4. Line current THD without and with shunt APF in M1 and M2

% THD of supply current	Without shunt APF	With Shunt APF M1	With Shunt APF M2
L1	**114.57**	**8.41**	**34.45**
L2	**98.63**	**7.17**	**18.82**
L3	**45.62**	**0.88**	**36.13**

For M1, the single phase V_S and I_L are initially converted to three-phase V_{abc} and I_{Labc} respectively by shifting the V_S and I_L by ±120º. Later on V_{abc} and I_{Labc} are converted into $V_{\alpha\beta0}$ and $I_{L\alpha\beta0}$ respectively by using conventional Clarke's transformation. Such transformation for L1 load current is shown in Fig. 12 and Fig. 13.

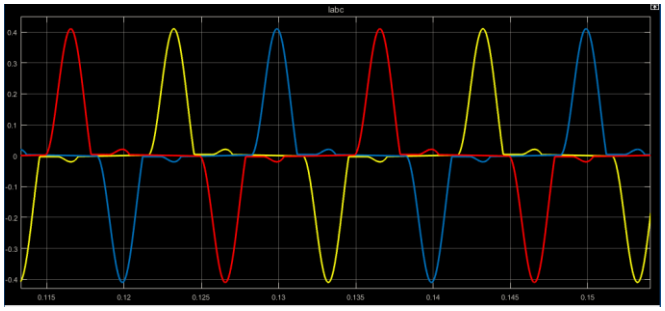

Fig. 12. M1 I_{Labc} waveforms before using Clarke's transformation for L1.

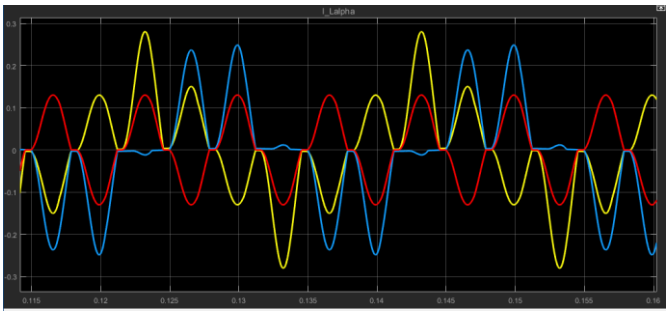

Fig. 13. M1 $I_{L\alpha\beta0}$ waveforms after using Clarke's transformation for L1.

For M2, the I_L is shifted at 90º transforming it into the $I_{L\alpha\beta}$ as shown in Fig. 14.

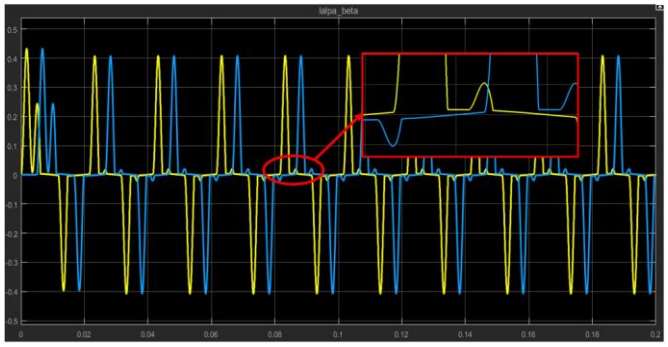

Fig. 14. M2 $I_{L\alpha\beta}$ waveforms after using phase shift for L1.

Even though both methods use same p and q calculation method, but the $I_{L\alpha\beta}$ for both M1 and M2 of L1 provided totally different waveform magnitudes, as shown in Fig. 15 and 16.

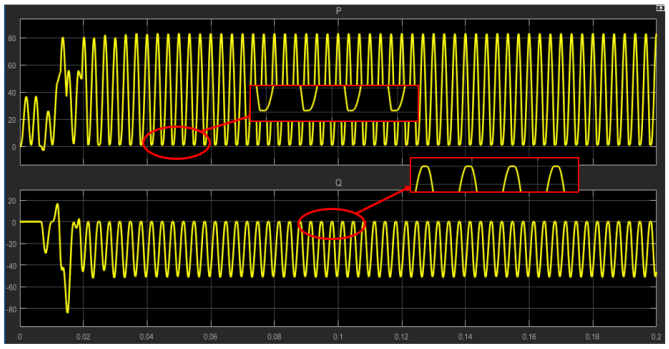

Fig. 15. M1 calculated p and q waveforms for L1.

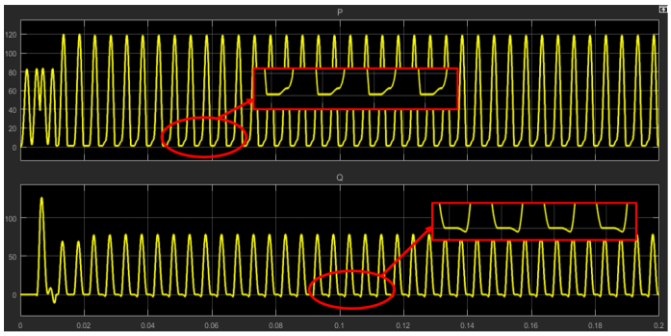

Fig. 16. M2 calculated p and q waveforms for L1.

The values of p and q play a main role for calculating the compensation current. For M1, in Fig. 15 the p and q signals are not touching the reference line therefore it does not possess zero crossing error. This is due to the Clarke's transformation, thus by converting distorted region in to the less distorted sinusoidal waveform. It is evident from Fig. 12 and Fig 13. However, for M2 it possesses the zero-crossing error. This condition occurs only for high harmonics distortion load for M2 because the $I_{L\alpha\beta}$ is exactly same as the load current. The distortion region between the $I_{L\alpha}$ and $I_{L\beta}$ caused the zero-crossing error at the signal p and q. This error is the main reason causing the error in the calculated HCC as shown in Fig. 17. The zero-crossing error tend to downgrade the performance of shunt APF.

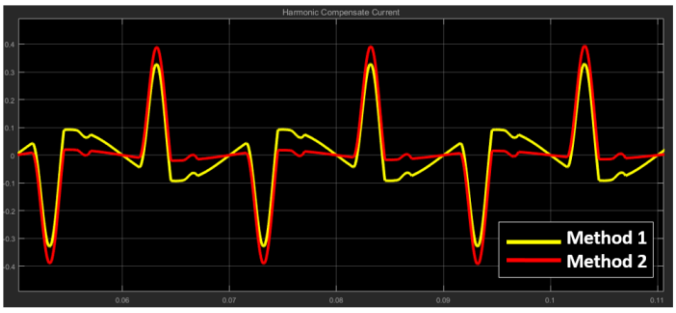

Fig. 17. The calculated HCC waveforms of M1 and M2 for L1.

Both L1 and L2 possess higher order harmonic. Therefore, the analysis for L2 will remain same. However, L3 is distinct by the even fashion of its harmonics. Since L3 only uses one diode for rectification so only half cycle of load current possessing high value of even harmonics is used. Fig. 18 and Fig. 19 show the I_{Labc} waveforms before Clarke's transformation and the $I_{L\alpha\beta0}$ waveforms after Clarke's transformation for M1 L3. However, Fig. 20 shows the $I_{L\alpha\beta}$ waveforms after phase shift for M2 L3.

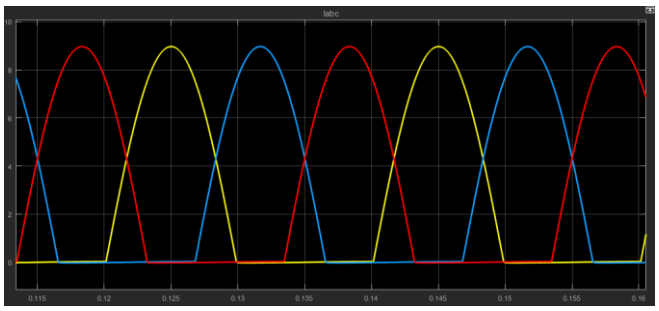

Fig.18. M1 I_{Labc} waveforms before Clarke's transformation for L3.

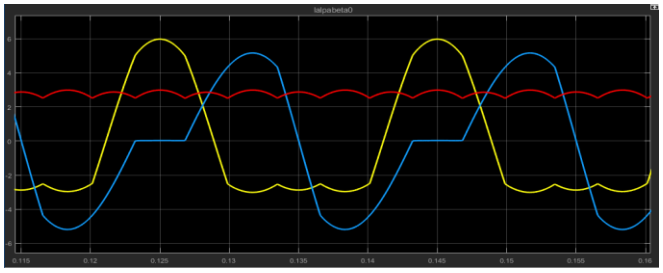

Fig. 19. M1 $I_{L\alpha\beta0}$ waveforms after Clarke's transformation for L3.

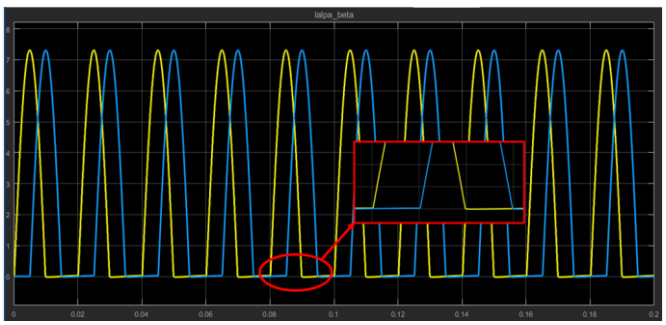

Fig. 20. M2 $I_{L\alpha\beta}$ waveforms after phase shift method for L3.

Figure 21 and Fig. 22 show the calculated p and q waveforms for M1 and M2 for L3. In M1 the p and q signal do not have the zero crossing error on the reference axis like M2. This condition occurs due to shifting the I_L to the $I_{L\alpha\beta}$, so

the $I_{L\alpha\beta}$ is exactly same as the load current. In Fig. 20, the distortion between $I_{L\alpha}$ and $I_{L\beta}$ is the main reason causing the zero crossing error at the p and q signal. Fig. 23 shows the calculated HCC waveforms of M1 and M2 for L3. This error causes the shunt APF not to compensate even harmonics and therefore tend to downgrade the performance of shunt APF.

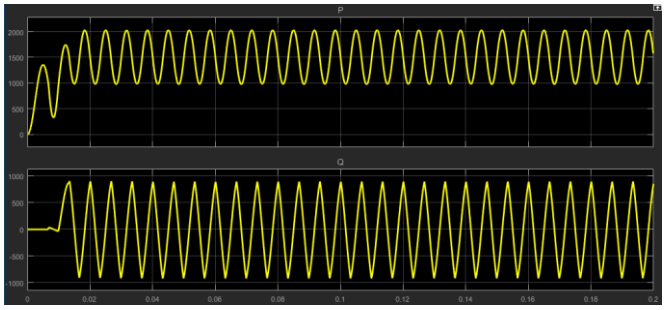

Fig. 21. M1 calculated p and q waveforms for L3.

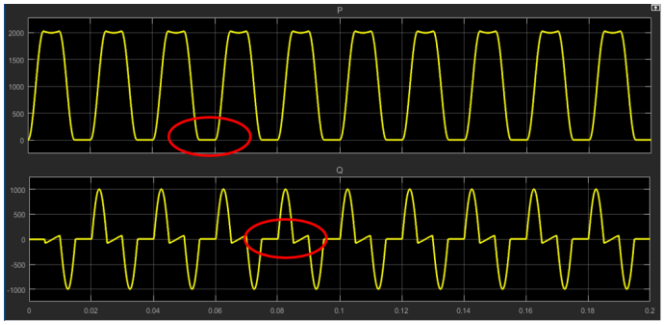

Fig. 22. M2 calculated p and q waveforms for L3.

Fig. 23. The calculated HCC waveforms of M1 and M2 for L3.

6. Conclusion

In this paper, the performance of shunt APF based on two methods of IRP theory: Clarke's transformation and Phase-shift method for single-phase system are investigated. Simulation results show the capability of both control methods for dealing with the current distortion under application of three different kinds of nonlinear loads. The shunt APF by using M1 Clarke's transformation is able to reduce the distortion current from 114.67 % (L1), 98.63 % (L2) and 45.62 % (L3) to 8.41 %, 7.17 % and 0.88 % respectively. The overall performance of M1 show the good harmonic compensation compared to M2 phase-shift method. M2 reduces the current THD of L1, L2 and L3 to 34.45 %, 18.82 % and 36.13 % respectively. This prove that the M2 is less effective for high distorted capacitive load like L1 and L2. It also unable to compensate even harmonics cause by L3. This situation is due to the distortion between the generated $I_{L\alpha}$ and $I_{L\beta}$ signals, causing the error in the calculated p and q values. Therefore, from the simulation results it can be concluded that M1 using Clarke's transformation given better harmonic compensate compared to M2 using phase shift method. Further analysis can carry out by constructing a prototype to testing both control methods with nonlinear loads to verify the simulation results.

References

[1] C. Venkatesh, D. S. Kumar, D. S. Sarma, and M. Sydulu, "Modelling of nonlinear loads and estimation of harmonics in industrial distribution system," in Fifteenth National Power Systems Conference (NPSC), IIT Bombay, 2008, pp. 592-597.

[2] P. R. Nasini and S. A. Narender Reddy Narra, "Modeling and harmonic analysis of domestic/industrial loads," 2012.

[3] R. J. Bravo and N. Y. Abed, "Experimental evaluation of the harmonic behavior of LED light bulb," in Power and Energy Society General Meeting (PES), 2013 IEEE, 2013, pp. 1-4.

[4] M. Khatri and A. Kumar, "Experimental Investigation of Harmonics in a Grid-Tied Solar Photovoltaic System," International Journal of Renewable Energy Research (IJRER), vol. 7, pp. 901-907, 2017.

[5] I. Ouerdani, A. B. B. Abdelghani, and I. S. Belkhodja, "Harmonic Analysis of Pulse Width Modulation-Based Strategies for Modular Multilevel Converter," International Journal of Renewable Energy Research (IJRER), vol. 6, pp. 838-846, 2016.

[6] F. Javernik, E. Hufnagl, M. Aigner, and E. Schmautzer, "The compliant integration of (renewable) power sources in MV or LV grids and the impact on grid reliability," in Renewable Energy Research and Applications (ICRERA), 2015 International Conference on, 2015, pp. 536-541.

[7] A. Y. Abdelazız, S. F. Mekhamer, and S. M. Ismael, "Technıcal consıderatıons ın harmonıc mıtıgatıon technıques applıed to the ındustrıal electrıcal power systems," presented at the 22nd International Conference on Electrical Distribution, 2013.

[8] J. Persson, "Comparing Harmonics Mitigation Techniques," 2014.

[9] M. Davudi, S. Torabzad, and B. Ojaghi, "Analysis of harmonics and harmonic mitigation methods in distribution systems," Australian Journal of Basic and Applied Sciences, vol. 5, pp. 996-1005, 2011.

[10] D. M. Soomro and M. Almelian, "Optimal design of a single tuned passive filter to mitigate harmonics in power frequency," 2015.

[11] M. Azri and N. Rahim, "Desıgn Analysıs Of Low-Pass Lc Passıve Fılter In Sıngle-Phase Grıd-Connected Transformerless Inverter," International Journal of Renewable Energy Resources (formerly International Journal of Renewable Energy Research), vol. 1, 2014.

[12] Y. Obulesu, M. V. Reddy, and Y. Kusumalatha, "A% THD analysis of industrial power distribution systems with active power filter-case studies," International Journal of Electrical Power & Energy Systems, vol. 60, pp. 107-120, 2014.

[13] M. Tarnini and A. Abdallah, "Analytical estimation in APF sizing for networks of analogous loads (Estimation of overall THD)," in Renewable Energy Research and Applications (ICRERA), 2015 International Conference on, 2015, pp. 124-128.

[14] O. Aissa, S. Moulahoum, I. Colak, B. Babes, and N. Kabache, "Analysis, design and real-time implementation of shunt active power filter for power quality improvement based on predictive direct power control," in Renewable Energy Research and Applications (ICRERA), 2016 IEEE International Conference on, 2016, pp. 79-84.

[15] A. Benyamina, S. Moulahoum, I. Colak, and R. Bayindir, "Hybrid fuzzy logic-artificial neural network controller for shunt active power filter," in Renewable Energy Research and Applications (ICRERA), 2016 IEEE International Conference on, 2016, pp. 837-844.

[16] A. Elgammal and D. Ali, "Self-Regulating Active Power Filter Compensation Scheme for Hybrid Photovoltaic-Fuel Cell Renewable Energy System for Smart Grid Applications," International Journal of Renewable Energy Research (IJRER), vol. 7, pp. 513-524, 2017.

[17] H. Akagi, "New trends in active filters for power conditioning," IEEE transactions on industry applications, vol. 32, pp. 1312-1322, 1996.

[18] R. C. Redondo, N. R. Melchor, M. Redondo, and F. R. Quintela, "Instantaneous active and reactive powers in electrical network theory: A review of some properties," International Journal of Electrical Power & Energy Systems, vol. 53, pp. 548-552, 2013.

[19] R. Pavlanin, M. Marinelli, and B. Zigmund, "Different view on pq theory used in the control algorithm of active power filters," Advances in Electrical and Electronic Engineering, vol. 5, p. 55, 2006.

[20] R. I. Bojoi, L. R. Limongi, D. Roiu, and A. Tenconi, "Enhanced power quality control strategy for single-phase inverters in distributed generation systems," IEEE Transactions on Power Electronics, vol. 26, pp. 798-806, 2011.

[21] M. Popescu, A. Bitoleanu, and V. Suru, "A DSP-based implementation of the pq theory in active power filtering under nonideal voltage conditions," IEEE Transactions on Industrial Informatics, vol. 9, pp. 880-889, 2013.

[22] M. Hamad, K. Ahmed, and A. Madi, "Current harmonics mitigation using a modular multilevel converter-based shunt active power filter," in Renewable Energy Research and Applications (ICRERA), 2016 IEEE International Conference on, 2016, pp. 755-759.

[23] E. Clarke, Circuit analysis of AC power systems vol. 1: Wiley, 1943.

[24] M. Aredes and E. H. Watanabe, "New control algorithms for series and shunt three-phase four-wire active power filters," IEEE Transactions on Power Delivery, vol. 10, pp. 1649-1656, 1995.

[25] T. Santos, J. Pinto, P. Neves, D. Gonçalves, and J. L. Afonso, "Comparison of three control theories for single-phase active power filters," in Industrial Electronics, 2009. IECON'09. 35th Annual Conference of IEEE, 2009, pp. 3637-3642.

[26] M. Priya and U. S. Balu, "Simulation results of a shunt active power filter using pq theory power components calculations," International Journal, vol. 2, 2014.

[27] P. Jintakosonwit, H. Fujita, and H. Akagi, "Control and performance of a fully-digital-controlled shunt active filter for installation on a power distribution system," IEEE Transactions on power electronics, vol. 17, pp. 132-140, 2002.

[28] H. Komurcugil, "Double-band hysteresis current-controlled single-phase shunt active filter for switching frequency mitigation," International Journal of Electrical Power & Energy Systems, vol. 69, pp. 131-140, 2015.

[29] R. Rao and S. S. Dash, "Power quality enhancement by unified power quality conditioner using ANN with hysteresis control," International Journal of Computer Applications, vol. 6, 2010.

[30] V. Khadkikar, "Enhancing electric power quality using UPQC: a comprehensive overview," IEEE transactions on Power Electronics, vol. 27, pp. 2284-2297, 2012.

[31] U. Dayaratne, S. Tennakoon, J. Knight, and N. Shammas, "Minimum DC link voltages for the generator bridge converter of a SCIG based variable speed wind turbine with fully rated converters," 2011.

[32] M. Vijayakumar and S. Vijayan, "A comparative study and ımplementation of controller for UPQC in single-phase to three-phase system."

[33] M. Vijayakumara and S. Vijayanb, "Photovoltaic based three-phase four-wire series hybrid active power filter for power quality improvement," Indian Journal of Engineering & Materials Science, vol. 21, pp. 358-370, 2014.

[34] H. Azevedo, J. Ferreira, A. J. de Pina Martins, and A. da Silva Carvalho, "Direct current control of an active power filter for harmonic elimination, power factor correction and load unbalancing compensation," Proceedings of the EPE 2003, 2003.

[35] N.-Y. Dai and M.-C. Wong, "Design considerations of coupling inductance for active power filters," in 2011 6th IEEE Conference on Industrial Electronics and Applications, 2011, pp. 1370-1375.

[36] F. Wu, S. Peng, and B. Wang, "The determination on DC capacitor parameter in active power filter," in The 2012 International Conference on Advanced Mechatronic Systems, 2012, pp. 265-268.

[37] S. C. Chong and D. M. Soomro, "Harmonic behavior of different branded LED lamps and their respective cost effectiveness," in 9th International Conference on Robotic, Vision, Signal Processing and Power Applications, 2017, pp. 725-736.

[38] R. N. Rao, "Harmonic analysis of small scale industrial loads and harmonic mitigation techniques in industrial distribution system," International Journal of Engineering Research and Applications, vol. 3, pp. 1511-1540, 2013.

[39] I. o. Electrical and E. Engineers, Standard IEEE Std 519-1992: IEEE Recommended Practices and Requirements for Harmonic Control in Electrical Power Systems: IEEE, 1993.

[40] G. Eduful, E. A. Jackson, and J. E. Cole, "Harmonic emission limits and selecting PCC location based on the type of distribution system," in Proceedings of the World Congress on Engineering, 2014.